Controllable generation of second-harmonic vortex beams through nonlinear supercell grating

Huijun Wang, Dunzhao Wei, Xiaoyi Xu, Mengying Wang, Guoxin Cui, Yanqing Lu, Yong Zhang, and Min Xiao

Controllable generation of second-harmonic vortex beams through nonlinear supercell grating

Huijun Wang,[1] Dunzhao Wei,[1] Xiaoyi Xu,[1] Mengying Wang,[1] Guoxin Cui,[1] Yanqing Lu,[1] Yong Zhang,[1,a)] and Min Xiao[1,2]

[1]*National Laboratory of Solid State Microstructures, College of Engineering and Applied Sciences, and School of Physics, Nanjing University, Nanjing 210093, China*
[2]*Department of Physics, University of Arkansas, Fayetteville, Arkansas 72701, USA*

Lithium niobate ($LiNbO_3$) nonlinear photonic crystals have been widely used in nonlinear wave front modulation for the π-phase difference between the second-harmonic (SH) waves from positive and negative domains. Aided by optimizing algorithms, we can control the diffraction patterns of SH vortex beams by designing nonlinear fork gratings with supercell structures in $LiNbO_3$ crystals. In experiment, we demonstrate that the diffraction energies can be equally distributed in each order or concentrated on certain orders, in agreement with theoretical designs. Potential applications include controllable vortex beam generation, nondestructive parallel vortex detection, and so on. *Published by AIP Publishing.* https://doi.org/10.1063/1.5050423

Light manipulation through a certain grating structure is crucial in many scientific areas such as optical communication,[1,2] photovoltaics,[3] sensing,[4] and imaging.[5] There are two extremes between which the optimal grating structure lies. They are random structures having numerous diffraction orders but are too weak and periodic structures that create insufficient diffraction orders. To address this issue, Martins and coworkers[6,7] proposed the concept of supercells to tailor the Fourier components of the periodic structures, i.e., large-period gratings consisting of small unit cells. The Fourier spectra of these gratings determine their optical diffraction properties. For example, gratings with a specially designed supercell may suppress unwanted diffraction orders,[8] shift the energy to higher orders,[6] and generate diffraction patterns with equal-power distributions as for Dammann gratings (DGs).[9]

Light beams featuring a helical wave front $e^{il\varphi}$, where l is an integer representing topological charge (TC) and φ is the azimuthal angle in the transverse plane, have been demonstrated to carry orbital angular momentum (OAM) of light.[10] Because of its unlimited bandwidth, donut-shape intensity distribution, and quantum properties, OAM has been studied thoroughly over the years in research fields such as optical communication, quantum information processing, and nonlinear optics.[11–16] Combining the fork grating with a supercell structure offers new degrees of freedom to manipulate vortex beams, which has potential applications in OAM multiplexing,[17] optical manipulation,[18] and volumetric optical vortex.[19] Until now, most of the light-manipulating gratings are fabricated with linear optical materials, for instance, photoresists,[20] silicon,[21] and liquid crystals.[22,23]

Lithium niobate ($LiNbO_3$) crystal,[24] a highly nonlinear crystal, has been widely used in optical frequency conversion,[25,26] nonlinear imaging,[27,28] nonlinear wave-front modulation,[29–31] and nonlinear OAM conversion.[14,15] Based on $LiNbO_3$ crystals, several nonlinear gratings have been recently proposed to manipulate light beams in a nonlinear way.[8,30,32] Conceivably, adapting the concept of supercell to design nonlinear fork gratings in a $LiNbO_3$ crystal can help engineer the diffracted nonlinear vortex beams.

In this letter, we experimentally demonstrate second-harmonic (SH) vortex-beam generation in an electrically poled $LiNbO_3$ crystal[33] using the concept of supercell. The supercell is designed to be a DG structure or optimized by genetic algorithm (GA) to control the nonlinear diffraction.[34] After coding the OAM information into the nonlinear DG, i.e., nonlinear Dammann vortex grating (DVG), we generate diffracted SH vortex beams with equal energies up to the first seven orders. The generated beams carry TCs from -3 to $+3$. Moreover, we use the GA optimized structure to selectively suppress or enhance certain diffraction orders. As an example, our experimental results show that the energy can be concentrated in the ±3-order SH vortex beams, while those of other orders are suppressed.

The first step is to design nonlinear supercell gratings for Gaussian beams. From the concept of the supercell, the diffraction beams can be controlled by changing the fine structure inside the supercell. For a one-dimensional periodic nonlinear grating in a $LiNbO_3$ crystal, the grating function (i.e., the distribution of nonlinear coefficient) has a Fourier series expansion

$$d_{22}(x) = \sum_m a_m \exp\left(i\frac{2\pi m}{\Lambda}x\right), \tag{1}$$

where Λ denotes the size of the supercell and a_m the m th Fourier component of the grating function, which depends on the structure of the supercell. In our experiments, we use an electrically poled z-cut $LiNbO_3$ crystal as the nonlinear grating, for which the positive and negative domains have nonlinear coefficients d_{22} and $-d_{22}$, respectively. The SH waves generated by the positive and negative domains

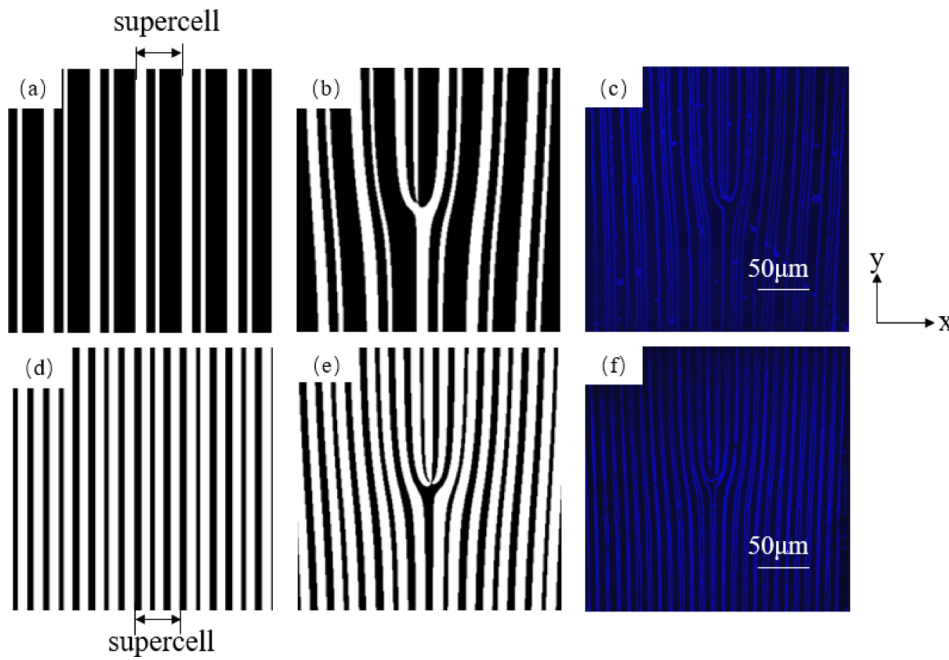a)Author to whom correspondence should be addressed: zhangyong@nju.edu.cn

FIG. 1. Phase structures of (a) DG, (b) energy-concentrated grating, (d) DVG, and (e) energy-concentrated vortex grating. The black and white stripes represent 0 and π phase, respectively. The size of one supercell unit is $\sim 27\,\mu$m in our experiment. (c) and (f) are the SH images of the DVG and the energy-concentrated vortex grating recorded using SH confocal microscopy.

have a phase difference of π, thereby forming a SH phase grating.[15] Figure 1(a) shows the phase structure of the nonlinear DG controlling seven diffraction orders. Within its supercell, the phase transitional points[35] between positive and negative domains (i.e., the relative positions of domain walls in a supercell) are 0.10, 0.29, and 0.53. This phase grating can shift the diffraction power of SH waves from low orders to high orders resulting in seven diffracted orders of equal powers. In principle, one can precisely tune the fine structure in the supercell to reconstruct the Fourier spectra and then produce the expected diffraction patterns. In our experiment, the optimization is performed based on GA. First, we divide one supercell into 20 units with randomly distributed nonlinear coefficients ($+d_{22}$ or $-d_{22}$). A population of randomly generated supercell structures forms the first generation. We numerically calculate the fitness of every structure in the population. The more fit structures are stochastically selected. After random crossover and mutation, a new generation of structures is formed for the next iteration of the algorithm. In our simulations, the algorithm is configured with a population of 100, a crossover probability of 0.8, and a mutation probability of 0.8. In order to improve the efficiency of numerical calculations, the evaluate fitness and constraint functions are all vectorized. With the above configurations of GA, the optimization of the supercell grating can usually be reached within 300 iterations. To centralize energy in the target orders, we calculate the best structure to realize the minimal value of the cost function[36]

$$C = aT + bE, \qquad (2)$$

where T denotes the probability of energy concentrated on unwanted orders, E the uniformity of the energy distributed on target orders, and a and b the weight coefficients. After optimization, we obtain transitional points of 0.1, 0.3, 0.45, 0.65, and 0.8 with the energy being concentrated in the ±3 diffraction orders [Fig. 1(d)].

The second step is to add the spiral phase of $e^{il\varphi}$ into the Fourier component of Eq. (1). We obtain a new distribution of the nonlinear coefficient expressed as

$$d'_{22}(x) = \sum_m a_m exp\left[im\left(\frac{2\pi}{\Lambda}x + l\varphi \right) \right], \qquad (3)$$

which determines a nonlinear fork grating with supercell. The m-order SH field is given by

$$E_m(2\omega) \propto E^2(\omega)a_m \exp\left[im\left(\frac{2\pi}{\Lambda}x + l\varphi \right) \right], \qquad (4)$$

where $E(\omega)$ is the fundamental field of the input beam. From Eq. (4), we see that the m-order SH beam carries topological charge of $m \times l$ with its energy proportional to $|a_m|^2$. Figures 1(b) and 1(e) show the designed nonlinear fork gratings by combining the spiral phase with the structures shown in Figs. 1(a) and 1(d), respectively. In our experiment, we choose $l = 1$, for example. We use SH confocal microscopy[37] to image the domain walls of the structured LiNbO$_3$ crystals [Figs. 1(c) and 1(f)].

The sample is fabricated by using an electric-field poling method.[38] To carry out the poling process, we first deposit a Cr electrode with a designed grating structure on the $+z$ face of the LiNbO$_3$ crystal and then apply an external electric field that is slightly larger than the coercive field of the LiNbO$_3$ crystal. The thickness of the LiNbO$_3$ sample is about 50 μm. The SH vortex-beam generation from a nonlinear supercell grating is achieved using an experimental setup shown in Fig. 2. A fundamental beam from a Ti:sapphire femtosecond laser (Chameleon, Coherent) with a pulse width of 75 fs and a repetition rate of 80 MHz passes through a half-wave plate and a polarizing beam splitter to control its power. The working wavelength is 900 nm. A lens with a focal length of 200 mm is used to focus the fundamental beam onto the sample. The diffracted SH beams are imaged by a CCD camera.
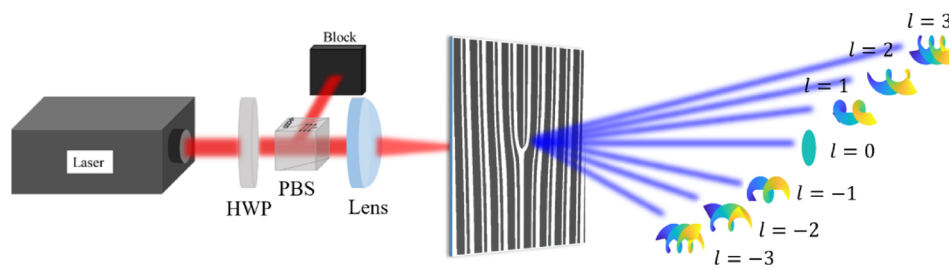
FIG. 2. Experimental setup. The fundamental beam of 900 nm from a femtosecond laser is controlled by a half-wave plate (HWP) and polarizing beam splitter (PBS) and focused on the sample by a lens. After filtering out the fundamental beam, the far-field SH patterns are captured by a charge coupled device (CCD). HWP: half-wave plate, PBS: polarizing beam splitter, CCD: charge coupled device.
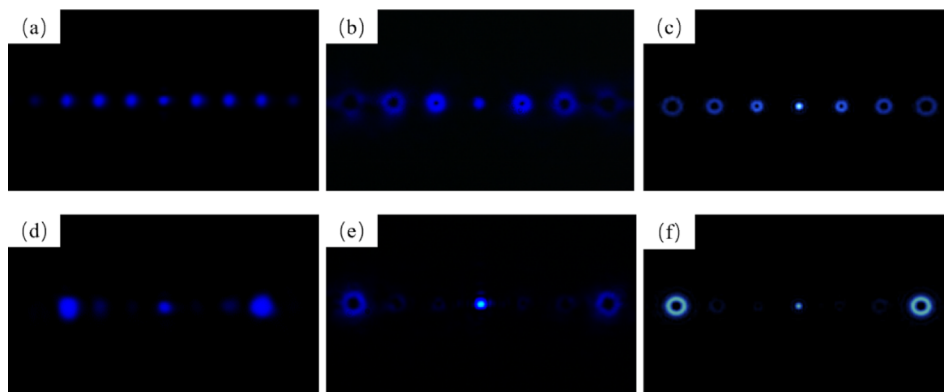

FIG. 3. SH diffracted patterns of (a) DG, (b) DVG, (d) energy-concentrated grating, and (e) energy-concentrated vortex gratings. (c) and (f) are the simulated patterns from ideal DVG and energy-concentrated vortex grating, respectively.

Figure 3(a) shows the diffraction pattern of the nonlinear DG for Gaussian beam manipulations [Fig. 1(a)] in which seven diffraction peaks are seen having nearly equal energies. The nonlinear DVG grating with $l = 1$ [Fig. 1(b)] generates seven diffracted SH vortex beams carrying topological charges from -3 to $+3$ [from left to right in c, Fig. 3(b)] as in the simulation [Fig. 3(c)]. Figure 3(d) gives the SH patterns concentrated in the ± 3th-orders by the GA-optimized grating for Gaussian beams. As expected, the majority of the power is concentrated in only two symmetric diffracted orders. Figure 3(e) shows the SH diffracted patterns generated by the OAM-coded nonlinear fork grating [Fig. 1(e)], by which the energy is concentrated in the ± 3-order vortex beams. As the loaded TC in the grating is $l = 1$, the output ± 3th-order SH vortex beams carry topological charges of ± 3 in accordance with Eq. (4). The experimental result in Fig. 3(e) agrees well with the simulation in Fig. 3(f).

For an intuitive understanding of the experimental results, we measure the energy of each diffracted order in Figs. 3(b) and 3(e). As shown in Fig. 4(a), the energy distribution from the nonlinear DVG is not perfectly uniform as

expected. Compared with the simulation of an ideal nonlinear DVG [Fig. 4(c)], the energy of the 0-order and ± 3th-orders in the experiment is diminished. For the nonlinear fork grating concentrating energies in ± 3th orders, the measured result [Fig. 4(b)] is very similar to the simulated one [Fig. 4(d)], except that the experimental 0-order power is slightly higher than the calculated value. The differences between the experiments and simulations are possibly due to fabrication errors during the electrical poling process, affecting not only the minimum line width but also the duty cycle. To confirm the cause, we use the measured nonlinear fork grating structures [Figs. 1(c) and 1(f)] to simulate the diffraction energy of every order. The obtained patterns [Figs. 4(e) and 4(f)] agree well with those from experiments [Figs. 4(a) and 4(b)]. To further optimize the nonlinear grating with the supercell structure, one should estimate fabrication tolerances beforehand, taking them into consideration in the design of the gratings.

In conclusion, we can control the energy distribution and topological charge of the SH vortex beam using a nonlinear fork grating with a supercell structure. By performing
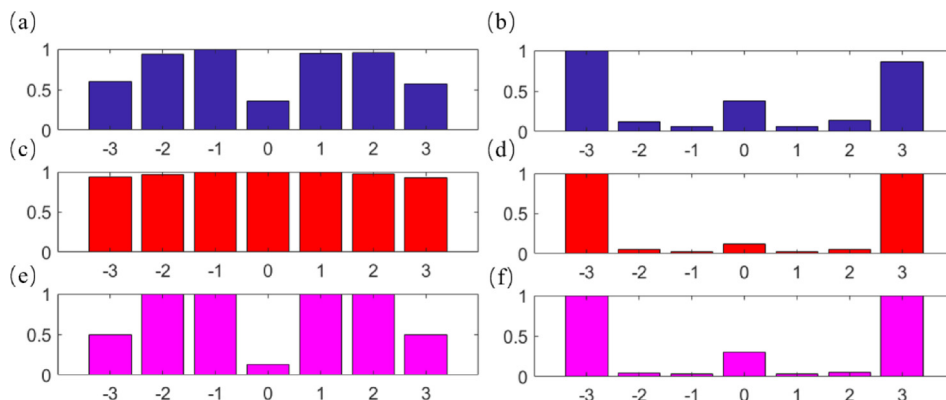

FIG. 4. (a) and (b) are the measured energies of each diffraction order in Figs. 3(b) and 3(e), respectively. (c) and (d) are the corresponding simulations of ideal gratings. (e) and (f) are the simulated results from the measured grating structures in Figs. 1(c) and 1(f), respectively.

SHG in the nonlinear gratings, we demonstrate the practicability of this method. Our method can be feasibly applied to higher-order OAM beams. Theoretically, applying GA optimization can concentrate the SH power into arbitrary diffracted orders carrying desired TCs, but one needs to consider fabrication errors in experiment. As a small change in wavelength only affects the emission angle slightly, such nonlinear grating can work as a wavelength-deviation-tolerant OAM generator. Moreover, nonlinear supercell grating is promising in nondestructive OAM detection[15,39] because it barely changes the wave front of the fundamental beam. These features make our method a potential candidate for applications in OAM-state parallel detection in optical communications, the generation of multiple arbitrary ultraviolet OAM modes for optical manipulation, and so on.

[1]V. R. Almeida, C. A. Barrios, R. R. Panepucci, and M. Lipson, Nature **431**, 1081 (2004).

[2]Z. Yu and S. Fan, Nat. Photonics **3**, 91 (2009).

[3]P. Bermel, C. Luo, L. Zeng, L. C. Kimerling, and J. D. Joannopoulos, Opt. Express **15**(25), 16986 (2007).

[4]S. Xiao, L. Zhang, D. Wei, F. Liu, Y. Zhang, and M. Xiao, Opt. Express **26**(2), 1997 (2018).

[5]S. Nie and S. R. Emory, Science **275**(5303), 1102 (1997).

[6]E. R. Martins, J. Li, Y. Liu, J. Zhou, and T. F. Krauss, Phys. Rev. B **86**(4), 041404 (2012).

[7]E. R. Martins, J. Li, Y. Liu, V. Depauw, Z. Chen, J. Zhou, and T. F. Krauss, Nat. Commun. **4**, 2665 (2013).

[8]C. R. Fernandez-Pousa and J. Capmany, IEEE Photonics Technol. Lett. **17**(5), 1037 (2005).

[9]H. Dammann and E. Klotz, Opt. Acta: Int. J. Opt. **24**(4), 505 (1977).

[10]L. Allen, M. W. Beijersbergen, R. J. Spreeuw, and J. P. Woerdman, Phys. Rev. A **45**(11), 8185 (1992).

[11]J. Wang, J. Y. Yang, I. M. Fazal, N. Ahmed, Y. Yan, H. Huang, Y. X. Ren, Y. Yue, S. Dolinar, M. Tur, and A. E. Willner, Nat. Photonics **6**(7), 488 (2012).

[12]A. M. Yao and M. J. Padgett, Adv. Opt. Photonics **3**(2), 161 (2011).

[13]A. Mair, A. Vaziri, G. Weihs, and A. Zeilinger, Nature **412**(6844), 313 (2001).

[14]Y. Wang, D. Wei, Y. Zhu, X. Huang, X. Fang, W. Zhong, Q. Wang, Y. Zhang, and M. Xiao, Appl. Phys. Lett. **109**(8), 081105 (2016).

[15]D. Wei, Y. Zhu, W. Zhong, G. Cui, H. Wang, Y. He, Y. Zhang, Y. Lu, and M. Xiao, Appl. Phys. Lett. **110**(26), 261104 (2017).

[16]X. Fang, Z. Kuang, P. Chen, H. Yang, Q. Li, W. Hu, Y. Lu, Y. Zhang, and M. Xiao, Opt. Lett. **42**(21), 4387 (2017).

[17]T. Lei, M. Zhang, Y. Li, P. Jia, G. N. Liu, X. Xu, Z. Li, C. Min, J. Lin, C. Yu, H. Niu, and X. Yuan, Light: Sci. Appl. **4**(3), e257 (2015).

[18]P. Chen, S. Ge, W. Duan, B. Wei, G. Cui, W. Hu, and Y. Q. Lu, ACS Photonics **4**(6), 1333 (2017).

[19]L. Huang, X. Song, B. Reineke, T. Li, X. Li, J. Liu, S. Zhang, Y. Wang, and T. Zentgraf, ACS Photonics **4**(2), 338 (2017).

[20]N. Zhang, X. C. Yuan, and R. E. Burge, Opt. Lett. **35**(20), 3495 (2010).

[21]G. M. Smolik and H. P. Herzig, Opt. Lett. **42**(16), 3233 (2017).

[22]F. Fan, L. Yao, X. Wang, L. Shi, A. Srivastava, V. Chigrinov, H. S. Kwok, and S. Wen, Crystals **7**(3), 79 (2017).

[23]P. Chen, S. J. Ge, L. L. Ma, W. Hu, V. Chigrinov, and Y. Q. Lu, Phys. Rev. Appl. **5**(4), 044009 (2016).

[24]N. G. Broderick, G. W. Ross, H. L. Offerhaus, D. J. Richardson, and D. C. Hanna, Phys. Rev. Lett. **84**(19), 4345 (2000).

[25]S. Zhu, Y. Y. Zhu, and N. B. Ming, Science **278**(5339), 843 (1997).

[26]H. Jin, P. Xu, X. W. Luo, H. Y. Leng, Y. X. Gong, W. J. Yu, M. L. Zhong, G. Zhao, and S. N. Zhu, Phys. Rev. Lett. **111**(2), 023603 (2013).

[27]Y. Zhang, J. Wen, S. N. Zhu, and M. Xiao, Phys. Rev. Lett. **104**(18), 183901 (2010).

[28]R. E. Lu, R. Z. Zhao, X. Feng, B. Yang, X. H. Hong, C. Zhang, Y. Q. Qin, and Y. Y. Zhu, Phys. Rev. Lett. **120**(6), 067601 (2018).

[29]T. Ellenbogen, N. V. Bloch, A. G. Padowicz, and A. Arie, Nat. Photonics **3**(7), 395 (2009).

[30]N. V. Bloch, K. Shemer, A. Shapira, R. Shiloh, I. Juwiler, and A. Arie, Phys. Rev. Lett. **108**(23), 233902 (2012).

[31]Y. Zhang, Z. D. Gao, Z. Qi, S. N. Zhu, and N. B. Ming, Phys. Rev. Lett. **100**(16), 163904 (2008).

[32]V. Berger, Phys. Rev. Lett. **81**(19), 4136 (1998).

[33]K. Mizuuchi, A. Morikawa, T. Sugita, and K. Yamamoto, J. Appl. Phys. **96**(11), 6585 (2004).

[34]Z. Chen, Y. Zhang, and M. Xiao, J. Opt. Soc. Am. B **32**(8), 1731 (2015).

[35]C. Di and C. Zhou, Appl. Opt. **45**(9), 1993 (2006).

[36]C. Zhou and L. Liu, Appl. Opt. **34**(26), 5961 (1995).

[37]X. Huang, D. Wei, Y. Wang, Y. Zhu, Y. Zhang, X. P. Hu, S. N. Zhu, and M. Xiao, J. Phys. D: Appl. Phys. **50**(48), 485105 (2017).

[38]G. X. Cui, Z. J. Wu, M. Y. Wang, Y. Ming, Z. Xing, K. Qiu, L. R. Yuan, J. Tan, X. J. Zhang, and Y. Q. Lu, Opt. Express **26**(4), 4194 (2018).

[39]D. Z. Wei, Y. M. Wang, D. M. Liu, Y. Z. Zhu, W. H. Zhong, X. Y. Fang, Y. Zhang, and M. Xiao, ACS Photonics **4**(4), 996 (2017).